

SIM astrometric demonstration at the 150 picometer level using the MAM testbed.

R. Goullioud, B. E. Hines, C. E. Bell, T. J. Shen, E. E. Bloemhof,
Jet Propulsion Laboratory, California Institute of Technology,
4800 Oak Grove Dr, m/s 171-113
Pasadena, CA91109
818 354 7908
renaud@jpl.nasa.gov

Abstract — Future space-based optical interferometers, such as the Space Interferometer Mission, require fringe measurements to the level of picometers in order to produce astrometric data at the micro-arc-second level. To be more specific, it is necessary to measure both the position of the starlight central fringe and the change in the internal optical path of the interferometer to a few tens of picometers. The internal path is measured with a small metrology beam whereas the starlight fringe position is estimated with a CCD sampling a large concentric annular beam. One major challenge for SIM is to align the metrology beam with the starlight beam to keep the consistency between these two sensors at the system level.

The Micro-Arcsecond Metrology testbed (MAM) developed at the Jet Propulsion Laboratory features an optical interferometer with a white light source, all major optical components of a stellar interferometer and heterodyne metrology sensors. The setup is installed inside a large vacuum chamber in order to mitigate the atmospheric and thermal disturbances. Recent data shows agreement between the metrology and starlight paths to better than 150pm in the narrow field of view of SIM. This paper describes the MAM optical setup, the alignment process, the current data and how the performance relates to SIM.

The MAM experiment is a key ground-based testbed that will demonstrate some critical technologies for SIM, the Space Interferometry Mission. SIM is discussed in more detail elsewhere in this volume [1], but is in essence a space-based Michelson interferometer that will carry out astrometry to micro-arcsecond precision on the visible light from a large sample of stars in our galaxy. SIM has a daunting list of technological challenges to address in order to show the mission is technically achievable. These challenges span from nanometer control problems to picometer sensing problems [2]. A number of system-level testbeds have been designed, built and tested thus far in the SIM's evolution. Each testbed is intended to address a system-level aspect of the SIM technology challenge. Examples of such testbeds include the Micro-Precision Interferometer testbed [3], the SIM Testbed 3 [4], and the KITE testbed [5]. The results from this collection of system testbeds will form the evidence that the technological challenges faced by SIM are solvable.

Interferometry of such high precision requires extremely accurate knowledge of interferometer baselines, and hence extremely precise internal metrology, which is to be carried out with near-infrared laser heterodyne metrology gauges working at the 1319 nm wavelength of Nd:YAG. For SIM to succeed, the optical path-length metric provided by the interferometer fringe determination must be faithfully tracked at the level of tens of picometers by the distances measured by metrology gauges, through all the operational motions of interferometer delay line and siderostats. The purpose of MAM is to demonstrate this agreement in a large-scale simulation that implements a substantial fraction of the final SIM flight baseline.

Figure 1 is a picture of the MAM experiment in the chamber that provides the vacuum necessary to obtain the required sub-nanometer performance. The MAM naturally divides into two distinct subsystems: the Test Article (TA), which is the interferometer proper, and the Inverse Interferometer Pseudo-Star (IIPS), which emulates a distant target star by providing spatially coherent wavefronts out of two mirrors, separated by the MAM baseline, that feed directly into the two siderostats of TA. The spectrum of the 600-1000 nm

TABLE OF CONTENTS

1. INTRODUCTION
 2. MAM TESTBED OVERVIEW
 3. SENSORS AND ACTUATORS
 4. ALIGNMENT
 5. PERFORMANCE METRICS
 6. DATA ANALYSIS
 7. RESULTS
 8. CONCLUSION
- ACKNOWLEDGEMENTS
REFERENCES

1. INTRODUCTION

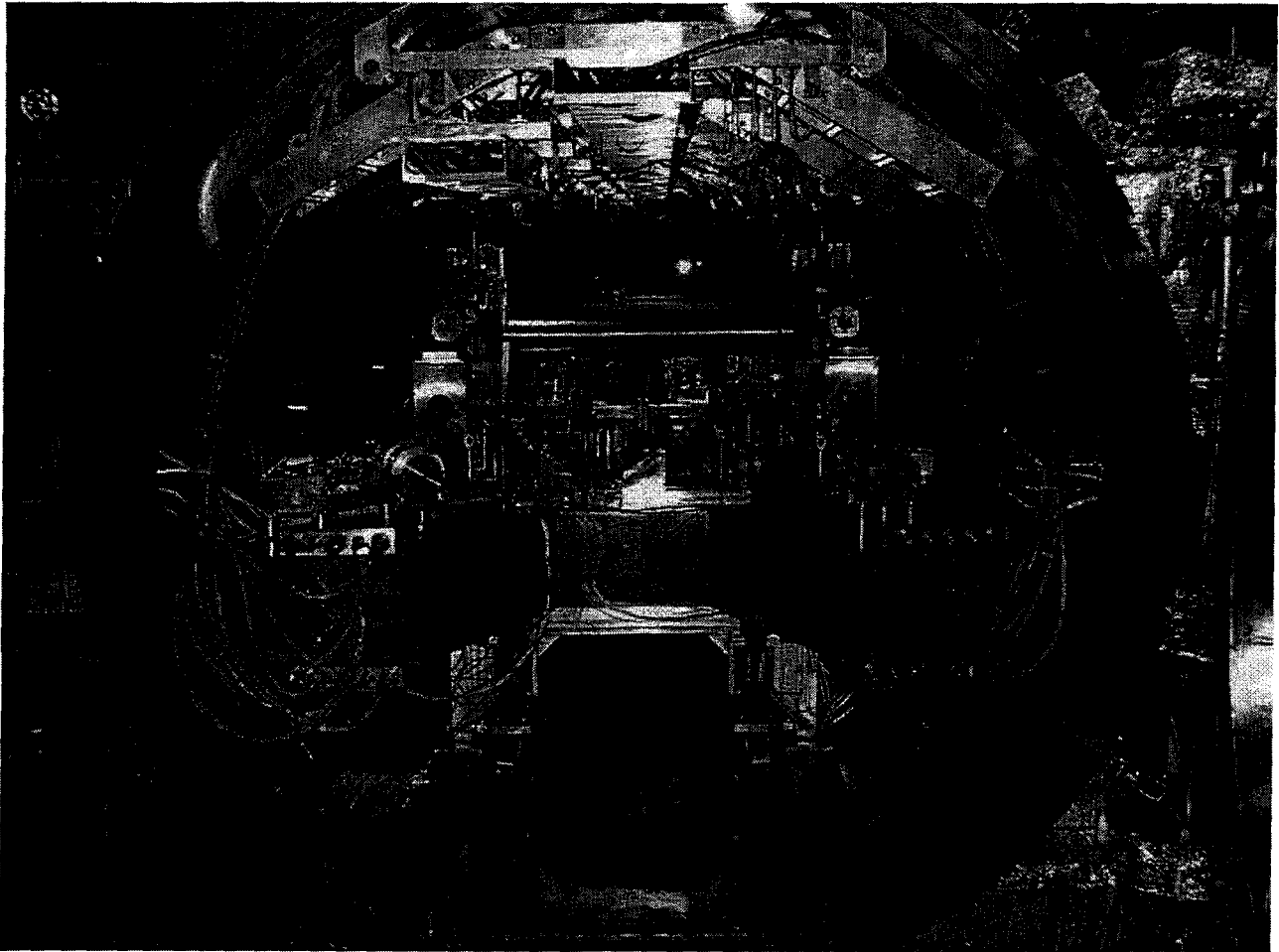


Figure 1 - The MAM experiment in the 45 foot long vacuum chamber.

white light ("starlight") generated by IIPS corresponds to that of a blackbody at a temperature of about 3100 K.

Figure 2 shows a schematic optical layout of MAM experiment. In addition to the central main beam combiner, which is the beam splitter at which light from the two arms of the interferometer are brought together to produce interference, TA contains a CCD camera to record fringes, a delay line to adjust the OPD between the two arms of the interferometer to the desired value, and a voice-coil modulator (VCM) to scan the OPD for fringe fitting. In addition to the white light source, IIPS contains a number of auxiliary light sources at different wavelengths that are used as beacons for alignment of system optics; also, one auxiliary light source provides an alternative metrology test (full aperture metrology, or FAM). Some of the technical details of MAM are discussed elsewhere in this volume [6], and some will be described more fully in later sections.

A severe technical constraint on the problem of tracking interferometry with metrology to picometer precision is faced by MAM as it will be by SIM: the starlight signal measured by the interferometer travels in an annular beam that fills most of the 40 cm siderostats, while the 1319 nm laser light for metrology travels in pencil beams located

within the "sub-aperture", or obscured 18 cm center, of these annuli, where they are directed to small reference corner cubes at the centers of the siderostats. The very different optical footprints of interferometry and metrology beams puts a premium on accurate optical alignment, which has motivated the development of the techniques discussed in this paper.

2. MAM TESTBED OVERVIEW

More precisely, the conceptual dividing line between TA, the interferometer, and IIPS, the light source that emulates spatially coherent white light from a distant star, is at the vertices of the two small corner cubes that are located within the sub-apertures of the two siderostats in TA. As part of the alignment procedure, the vertices are arranged to be precisely coincident with the rotation axes of those siderostats. Metrology gauge launchers in both TA and IIPS measure round-trip distances, with precision in the neighborhood of 10 pm, to and from the vertices of these corner cubes; for this reason, the launcher in this scheme is designated SAVV, for Sub-Aperture Vertex-to-Vertex. Zhao et al.[7] present details and stand-alone performance of

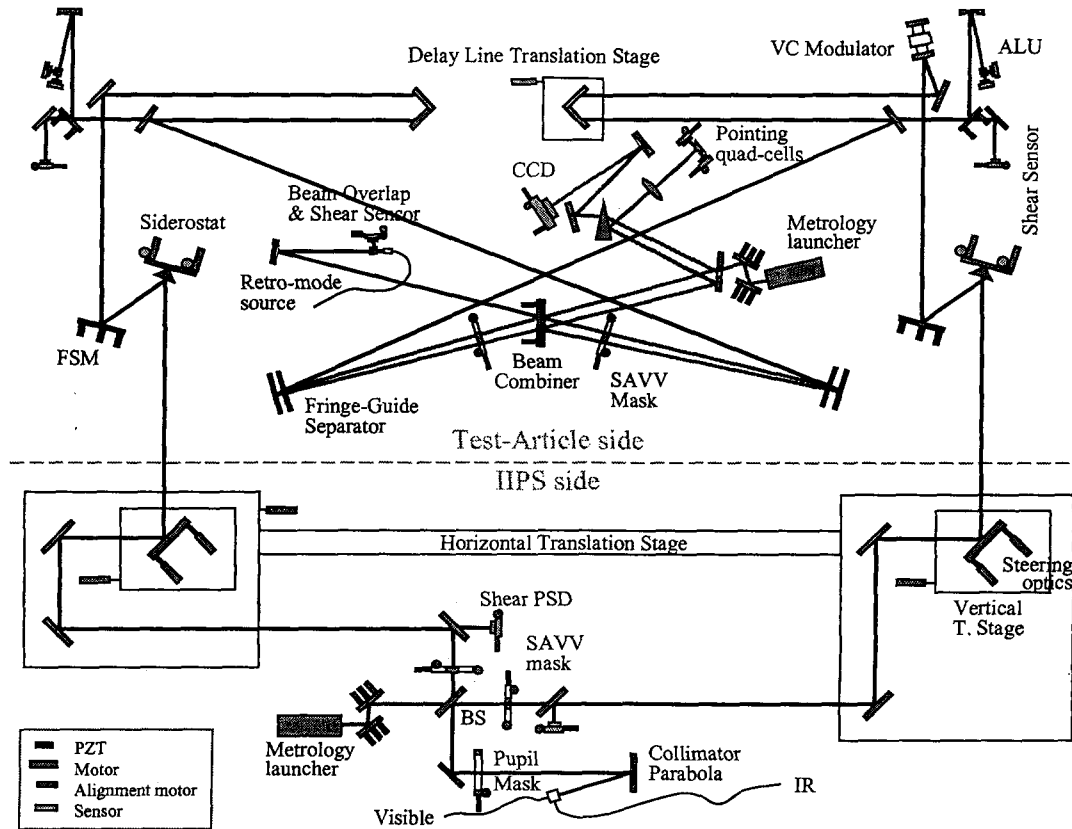


Figure 2 - MAM main optical layout.

the SAVV metrology launcher. Placing the vertices on the siderostat rotation axes is clearly a first step to maintaining agreement between starlight and metrology OPDs, as the siderostats are moved in pointing angle to carry out “field dependent” tests that simulate observations of multiple stars with SIM.

There is one difference between TA and IIPS regarding how the metrology beams are handled. The “metrology launchers” on each subsystem are capable of launching and receiving 1319 nm metrology light, but on the IIPS side metrology light may also be introduced via the cube beam splitter near the bottom of Figure 2. There, white “starlight” and the various auxiliary beacons plus FAM are introduced on the fiber labeled “Visible”, to be combined with 1319 nm metrology radiation introduced on the fiber labeled “IR”. Launching starlight and metrology light from a single source in this way permits co-alignment of the beams to high accuracy. This separation of metrology beam launch from metrology reception and heterodyne detection, which still occur in the “metrology launcher” box, is termed “split-SAVV” mode.

The starlight and metrology beams emerge from the cube beam splitter in IIPS with beam patterns typical of launching into free space from bare fibers, $\sim f/8$ or so, and they are collimated by an off-axis paraboloid (Figure 2) before being directed to the main beam splitter (BS) that will divide the beams for the two output arms of IIPS. A set of two

compensating beam splitters, with substrates and coatings identical to those of the main beam splitter, maintains uniformity between the two arms by ensuring that each path experiences both a transmission and a reflection. A “pupil” mask defines the annular beam for starlight. “SAVV” masks, different in each arm of IIPS, define the sub-aperture metrology beams; these are configured as sets of two square pencil beams in the inner part of the annulus, with the pencils stacked vertically in one arm and horizontally in the other arm of IIPS. The output beams, the outer, annular (“full-aperture”) starlight beam with inner, “sub-aperture” pencil beams of 1319 nm metrology light, are sent from two IIPS steering mirrors directly opposite TA’s two siderostats. To accommodate motions of the siderostats that emulate observations of multiple stars at different field positions, the IIPS steering mirrors are mounted on translation stages whose motions are determined as part of the alignment procedure.

The starlight beam, before injection into the cube beam splitter for combination with metrology light, has been combined with laser beacons at 532, 633, and 980 nm that are used in the alignment procedure. Also included is the full-aperture metrology (FAM) signal, an annular beam at 660 nm that is obtained by frequency doubling in a non-linear crystal from the same laser source that delivers 1319 nm light for metrology. Optimum performance of IIPS, which has requirements on wavefront quality over one output beam ($\sim \lambda/4$) and uniformity between the two arms

($\lambda/10$), requires accurate co-alignment of starlight and metrology beams in both tip/tilt and shear. Shear detectors (labeled "Shear PSD" in Figure 2), which are mounted behind the compensating beam splitters, will be used for this determination.

At the TA siderostats, the starlight signal passes through for fringe measurement by TA, the interferometer proper. The metrology light originating in IIPS is retro-reflected and retraces its path through the IIPS optics until it is returned to the metrology box shown in Figure 2 for heterodyne detection. A corresponding pair of sub-aperture metrology beams originates in the metrology launcher in TA, and measures the round-trip distances along the two arms of the interferometer between the launcher and the same corner-cube vertices. In this way the complete optical path traversed by starlight is measured by metrology, in two pieces. The siderostats control gross pointing, but they are fed by fast-steering mirrors (FSMs), which carry out high-bandwidth tip-tilt corrections to lock the peak of the starlight signal onto a certain position on the CCD. The FSM control loops are closed with a signal derived from the blue portion of the starlight beam, which is diverted by the "fringe-guide separators" in Figure 2 and directed into the "pointing quad-cells". Figure 2 shows an auxiliary light injection source on TA, the "retro-mode source", that is not used in standard operation of the testbed, but allows preliminary tests of TA operation without the IIPS pseudo star. In this mode, the starlight injected by the retro-mode source traverses the optics of TA in a roundtrip, to and from a pair of special corner cubes positioned in front of the siderostats.

3. SENSORS AND ACTUATORS

White light detector: CCD

The central sensor in MAM is the CCD camera, a small-format (40x40) silicon device used to monitor fringes in the white-light beam as the interferometer OPD is scanned a few wavelengths by the voice-coil modulator (VCM). Owing to the prism disperser that precedes it, the CCD camera has one spatial and one spectral dimension. The spectral dimension covers roughly 600-1000 nm, encompassing the auxiliary HeNe metrology beam at 633 nm or the FAM at 660 nm, and most of the light emitted by the white-light (starlight) source, a 3100 K blackbody.

Metrology detector

Heterodyne detection for metrology is done within the boxes labeled "metrology launcher" in Figure 2. There are two independent launchers on the TA and on the IIPS side of MAM. Each launcher sends out two independent sets of dual measurement beams that traverse the two arms of TA or IIPS, where they are ultimately retro-reflected from the small corner cubes mounted in the sub-aperture of the two siderostats. The roundtrip distance is measured by

heterodyne interferometry against a reference beam (local oscillator, or "LO") that is kept physically confined within each launcher. Measurement and reference beams are coherent, but shifted in frequency by a small amount (~40 MHz). The measurement beams are sent out in pairs as square pencil beams, 3.5 mm on a side, within the sub-aperture. The SAVV masks, located as shown in Figure 2, ensure that the beams for one arm are arranged side by side (horizontally), and for the other are stacked vertically, so there is no confusion between the two heterodyne signals. The final detection for the two arms is made by two distinct photodetectors within the launcher.

Alignment quad-cells and shear sensors

A number of sensors have been built into MAM specifically to monitor optical alignment, and a number of actuators have been implemented to make the adjustments to the alignment that are indicated by the readings of those sensors. Sensors generally measure pointing (tip/tilt) or beam shear; these may be accomplished with quadrant detectors ("quad-cells") at a focal plane or at a pupil plane, respectively. MAM uses two kinds of quad-cells: silicon detectors that are sensitive to visible light at wavelengths shorter than about one micron, and InGaAs detectors that are sensitive to the near-infrared (specifically, to 1319 nm metrology radiation) and to wavelengths as short as just below one micron. Formal centroid accuracy is very high, if only photon signal-to-noise ratio is considered, but irregularities in detector properties (e.g. spatial variations in quantum efficiency) limit the accuracy in practice.

Boresight Alignment Unit (ALU)

Alignment units (ALU) were developed for the MAM experiment by the Lockheed-Martin Missiles and Space Corporation, Advanced Technology Center, in Palo Alto, CA. Figure 3 shows one Alignment Unit. They are quad-cells at the focal plane of a collimating mirror having a focal length of one meter, so they are sensitive to the tip/tilt alignment of a beam. ALUs are located on both arms of TA (see Figure 2 and Figure 6). Each ALU has a dichroic that splits infrared light (primarily from the 1319 nm metrology beam) from visible light (primarily from the interferometer white light), which are then sensed by Si and InGaAs detectors, respectively, so the visible and IR beams may be boresighted with respect to each other. The initial relative alignment of the Si with the InGaAs detectors is established with a 980 nm laser diode, seen by both detectors.

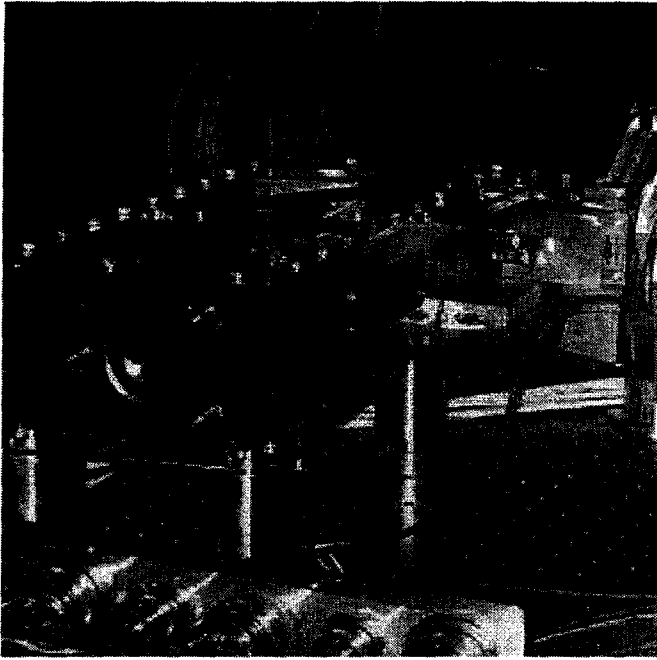


Figure 3 - Alignment Unit: the two detectors are the two gold rectangular boxes on the right side of the picture.

Siderostats

A fundamental actuation in MAM is motion of the siderostats to simulate observations of multiple stellar targets by a space-based interferometer like SIM. Figure 4 shows one of the two siderostats. IIPS, the artificial star, must make corresponding motions of its two output mirrors, directly opposite the two siderostats of TA, and so these are mounted on vertical translation stages that are mounted on a ganged horizontal translation stage.



Figure 4 - MAM siderostat with corner-cube at the center of the optics.

Because the corner cube at the center of the siderostat mirror has its vertex in the plane of the gimballed axes, the siderostat

can be moved without affecting the OPD measured by the metrology beams.

Pupil mask

The annular pupil of the starlight beam that runs through the IIPS pseudo-star and then through the TA interferometer must be defined by masking somewhere in the system, since the visible-light injection via the cube beam splitter has only the free-space output pattern of an optical fiber to define it. We have chosen to locate the pupil mask on the IIPS side of MAM, close to the originating light source (see Figure 2 and Figure 6). A central issue in the co-alignment of white light with the 1319 nm metrology pencil beams is shifting the pupil mask to shift the location of the white light photometer, and thus minimize the relative shear with metrology.

Actuators

MAM must be operated in a vacuum chamber to minimize the large errors induced by atmospheric turbulence that will be quite different for full-aperture white light and sub-aperture metrology, so remote motorized control of the many adjustable subsystems is required. For operating a system as complex as MAM, highly automated and rapid control of the alignment procedures is a practical necessity as well. Figure 2 gives a schematic indication of the motors that drive some of the key actuators; many others are not shown.

Piezo-electric drives (PZTs) are used when smooth, fast motions over relatively short strokes are required, as with the FSMs and the IIPS steering mirrors. The IIPS steering mirrors also have a second stage of motors, Burleigh Inchworms, which are also piezo-electrically driven. Encoded servo-motors from Oriel are used to drive the siderostats and the actuators that translate the pupil mask. Stepper motors are used to drive the interferometer delay line on the Test Article side, and the translation stage that moves the steering mirror towers on the IIPS side. Motorized adjustment screws from New Focus, called "picomotors", are used for a number of remaining functions of a less precise nature that must be actuated in MAM, where repeatability is not an issue. Finally, DC motors are used to move masks in and out of the beams. All motors must, of course, be vacuum compatible. The PZT-based models, but particularly the Burleigh Inchworms, are susceptible to damage in a certain range of pressures, about 1 to 1000 milli-Torr, the "corona" region, over which these relatively high-voltage devices will arc.

4. ALIGNMENT

The challenge of the MAM experiment is to measure the same path using two separate and quite different optical probes. The heterodyne metrology gauge uses a compact,

bright and highly coherent laser beam. Therefore, one can expect high resolution measurements. The starlight sensor collects a larger, weaker beam from a faint, incoherent source (a nearby star for SIM, or a light bulb coupled to a fiber for MAM). To maximize the amount of starlight collected, the sub-aperture metrology beam must be as compact as possible. The two beams are concentric, but they do not overlap. Also, to avoid cross-contamination of the two light beams, metrology is carried out at a much different wavelength (1.3 μm) than is used for starlight observations (the 0.6 to 1.0 μm band). The metrology beam uses the central portion of the optics and retro-reflects on the corner-cube, so as to travel a roundtrip through the MAM optics. The starlight reflects on the annular portion of the optics and travels only once through the optical train. Finally, the pathlength estimation from the heterodyne metrology sensor and the dispersed fringe sensor will have different errors specific to these very different techniques.

In summary, there are many known reasons why infrared metrology and white light (starlight) interferometry will disagree. The wavelength difference will cause dispersion-related errors that are very sensitive to thermal effects. Diffraction effects will be quite different for metrology and starlight, an issue that is addressed in the diffraction testbed experiment [8]. Beam walk on the optics will cause errors due to imperfect wavefront quality: even an optic figured to 1/100 of a wave RMS has surface irregularities of 6000 pm rms. As the small metrology beam moves around, or “walks”, on this surface, the path length difference between metrology and starlight will change [9]. In the current study, we are addressing one of the potentially largest sources of error in MAM: imperfect geometric alignment between the metrology and starlight beams.

Requirements

The starlight beam is emitted by the pseudostar, collected by the siderostats, and detected in the spectrometer. The metrology beam is issued by the launcher, retro-reflected on a corner-cube, and detected back in the launcher. Where the metrology and the starlight beams share the same optics, they have to measure the pathlength with an accuracy of a few picometers. Even with the best effort, the two concentric beams are not precisely concentric; indeed, they will be offset laterally by a distance S (shear). The two beams will be approximately parallel, with a small residual tilt ϕ . At the recombination (see Figure 5), the two beams will have traveled to the first order the same path with a slight difference $d = S \cdot \phi$. If ϕ is only 10 micro-radians (2 arc-seconds) and S is only 100 microns, the pathlength difference is $10 \mu\text{rad} \cdot 100 \mu\text{m} = 1000 \text{ pm}$ (picometers).

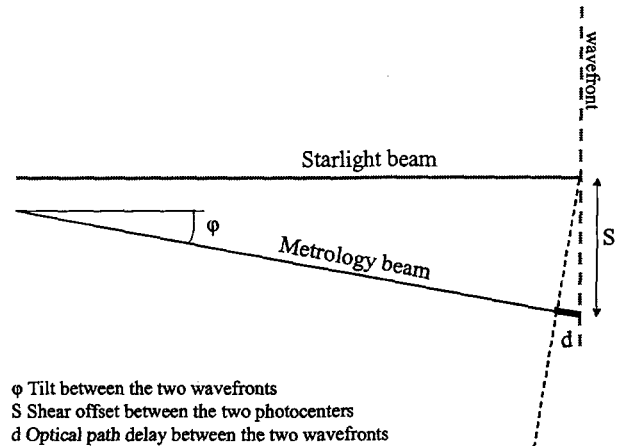


Figure 5 - Pathlength error due to misalignment between the metrology beam and the starlight

However, the metrology is only a relative sensor tracking changes in optical path. Therefore, an absolute delay of a few hundred picometers over meters of optical path is not an issue. The real issue is changes in the delay. If the tilt changes by $\Delta\phi$, the delay between the metrology and the starlight paths will change by $\Delta d = S \cdot \Delta\phi$. Conversely, a slight shear of the metrology beam relative to the starlight beam, by ΔS , will cause an error in the path measurement $\Delta d = \phi \cdot \Delta S$. Note that, if the absolute tilt between the metrology and the starlight wavefront ϕ is small to start with, the sensitivity to shear jitter and drift ΔS is small. Similarly, if the absolute shear between the two concentric beams S is small, the sensitivity to the tilt jitter and drift $\Delta\phi$ is smaller too. Therefore, it is critical to optimize the absolute tilt and overlap alignment between the metrology and the starlight beams.

We have to be concerned about the absolute tilts and shears among the starlight beam, the metrology measurement beam and the metrology local oscillator, on both the Pseudo-Star side and the Test-Article side of MAM. There is a dozen error sources related to initial alignment alone; the allocation table (Table 1) shows the detailed error budgeted to each of them. Even though only 20 pm are allocated for the MAM alignment error budget, Table 1 shows a total of 270 pm. The main reason is that the two numbers refer to different averaging times. The 20 pm requirement assumes the 10-chop observing scenario planned for SIM, in which the linear drift from one 30 second chop to the next is removed. The 270 pm allocation corresponds to raw measurements uncorrected for drift, spanning 15 minutes or so.

Table 1 - Detailed error allocation.

MAM Optical Alignment Term	Static shear (μm)	Tilt drift (μrad)	Static tilt (μrad)	Shear drift (μm)	Error (pm)
IIPS, metrology (Measure/LO) tip/tilt			16	2	32
TA, metrology (Measure/LO) tip/tilt			16	5	80
IIPS, metrology (Measure/LO) shear	100	0.05			5
TA, metrology (Measure/LO) shear	100	0.05			5
IIPS, starlight vs metrology tip/tilt			5	2	10
TA, starlight vs metrology tip/tilt			30	5	150
North/South arms tip/tilt			4	8	32
Starlight vs metrology shear	200	1			200
TOTAL:					270

The alignment procedure for MAM is necessarily complex, but there are some simple underlying tactical themes. The vertices of the corner cubes mounted on the sub-apertures of the two siderostats mark the precise dividing line between TA and IIPS (see Figure 6). Alignment of TA metrology and IIPS metrology are independent problems, of course, as each gauge measures roundtrip distances to the vertices from opposite directions. But alignment of the starlight used for the interferometer is highly coupled. For starlight, alignment generally begins at the light source in IIPS and work down the optical paths toward the sensors in TA. For both starlight and metrology, it is generally advantageous to accomplish tip/tilt alignment of two beams first, and then beam shear and/or overlap from the two arms.

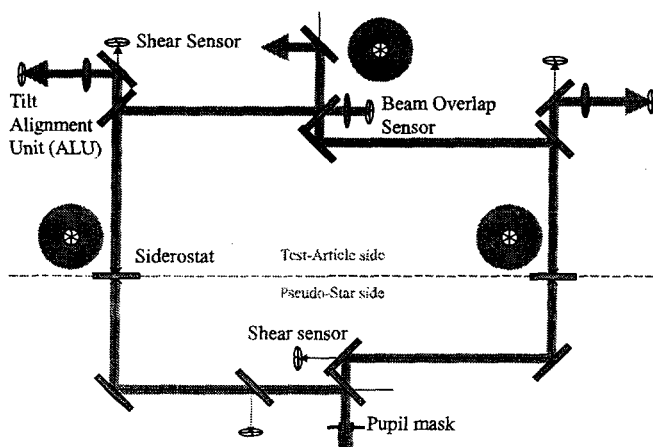


Figure 6 - Alignment sensors

While Figure 6 provides a schematic overview, there are many motorized actuators and auxiliary sensors not shown. These include motorized shutters, pupil masks, metrology masks, and quadrant detectors (some also motorized), some configured as tip/tilt sensors and some as beam shear

sensors. Some have been briefly described in previous sections.

TA (Test Article) metrology

The first step in aligning the 1319 nm metrology beam in TA is an internal adjustment of the metrology gauge itself. The gauge is a heterodyne interferometer that compares a “measurement” beam, which is sent out to traverse a roundtrip through the TA optics, to a “reference” or local oscillator (LO) beam, coherent but slightly shifted in frequency, that remains within the launcher. The two beams pass through an internal set of Risley prisms that have been adjusted to minimize beam shear. A corner cube is then inserted by a motorized actuator in front of the launcher, so the measurement beam is retro-reflected and the relative tip/tilt between it and the internal LO beam may be adjusted with motorized wedges driven by picomotors. A unique feature of the SAVV metrology launcher is that it sends out two independent measurement beams to traverse the two arms of the interferometer, though only a single LO beam is used by both. The tip/tilt adjustment is done to maximize the metrology signal amplitudes, and to keep the two independent metrology signals in phase, ensuring equal paths within the metrology gauge.

Now the motorized corner cube is removed, and the measurement beams are sent out to the two corner cubes mounted in the sub-apertures of the two siderostats. SAVV masks keep the beams traversing the two arms of the interferometer separate, so two distinct heterodyne signals are produced by two photodetectors within the metrology launcher. The metrology signal amplitude for one arm (the South arm) is maximized by moving the flat mirrors arranged as a periscope in front of the launcher; these are motorized with picomotors. The effect of moving the periscope mirrors is to translate the metrology beam on the siderostat corner cube, and maximum signal should occur when that beam is centered on the corner cube vertex. When the South arm alignment is completed, the metrology signal amplitude for the other (North) arm is maximized by tilting the main beam combiner in TA, which is motorized with picomotors.

Now that the metrology beams have been established on both arms of TA, the infrared shear sensors (quad-cells) are adjusted in transverse position to put one of the dual metrology spots at their centers. Each quad-cell is mounted on a translation stage, driven by picomotors, to simplify this adjustment.

IIPS (Pseudo Star) metrology

The operation of the metrology gauge in IIPS, measuring the roundtrip distance from the launcher to the corner cubes mounted in the sub-aperture of the TA siderostats, is very similar to that of the gauge in TA, and the alignment procedures are similar as well. As before, an auxiliary corner cube on an actuated shutter is inserted in the beam

immediately in front of the launcher, and wedges motorized with picomotors are used to adjust the tip/tilt between measured and LO beams until a maximum of the heterodyne metrology signal is achieved.

The next alignment step makes use of the so-called “split-SAVV” beam, which is the coherent 1319 nm metrology (“IR”) beam launched from the cube beam splitter along with the starlight beam in Figure 2. Because it is injected identically, split-SAVV is a useful tracer for starlight. This fact is exploited by disconnecting the IR fiber that usually injects LO power into the metrology launcher, and moving it to inject the IR light via the cube beam splitter. The LO-powered split-SAVV beam thus produced will interfere with the two measurement beams sent out in the usual way by the metrology launcher, and produce heterodyne signals for each arm of IIPS. These signals are maximized for each arm by adjusting the tip/tilt of the flat mirrors in the periscope adjacent to the launcher. There are several local maxima in a two-dimensional envelope, but the central maximum, where the two metrology signals are in phase, giving equal paths on the two arms, must be found. When this is accomplished, parallelism will be established between the metrology measurement beam and the starlight beam, which the split-SAVV beam has been emulating; the IR fiber is then returned to its standard position, delivering LO power to the metrology launcher.

We next maximize the metrology signal amplitude for the South arm by tilting the IIPS steering mirror on that arm. This will have the effect of translating the metrology beam on the corner cube mounted in the sub-aperture of the TA siderostat, and a maximum return signal will correspond to minimizing the shear of the measurement beam with respect to the corner cube vertex (i.e. centering it). This shear alignment is then repeated for the North arm using the other IIPS steering mirror.

The final adjustment for the IIPS metrology system is moving the shear sensors laterally until the metrology beams are at the null positions of the quad-cells. These shear sensors are also motorized, with picomotor-driven translation stages. Since the shear sensor quad-cell will define the reference position to maintain alignment while the artificial star is articulated through the 1 degree field required for “narrow-angle field-dependent” MAM tests, it is critical to adjust their position properly.

Starlight/Metrology parallelism

Parallelism alignment between metrology light and starlight was accomplished on the IIPS side of the experiment as part of the metrology alignment of the previous section. On the TA side, this alignment is carried out with the Alignment Unit (ALU). On each arm, the ALU feed mirror is adjusted to put the TA metrology spots on the IR quad-cells at the null positions. Then, again independently on each arm, the 532 nm green laser beacon is used as a tracer for the

starlight beam, and is brought to the null position of the corresponding visible-light ALU quad-cell by moving the siderostat on that arm. It is now possible to servo the fast-steering mirrors (FSMs) on each arm using drive signals derived from the green laser beacon on the appropriate ALU visible-light quad-cell.

Pointing loop reference

For this alignment, the FSM pointing loops must be kept closed on the initial targets that were set during the TA alignment described in the previous section. (Large steady-state deflections of the FSMs as the system drifts must be offloaded to the siderostats, to avoid shear of the metrology beams on the siderostat corner cubes.) In addition to the green laser beacon, the HeNe laser that is injected with the starlight source via the cube beam splitter in IIPS is turned on. The HeNe beam will form a spot on the CCD in TA, and picomotor-driven translation stages are used to center that spot on the target location that gives the correct shift to image the entire spectral range needed by MAM. If the interferometer OPD is scanned by the voice coil modulator (VCM), the HeNe spot will vary in intensity and a fringe visibility may be derived. This visibility is maximized by adjusting the offset of the North-arm FSM, within the feedback loop that is kept closed. When this is done, the final pointing target that will maintain high-visibility fringes has been established.

Starlight/Metrology overlap in shear (the “pointing decenter” test)

There is no easy way to directly adjust the starlight and metrology beam shear, as device variations over the face of a quad-cell limit the practical precision to which the center of a large-diameter beam defining a pupil may be found. However, we may use the OPD signature from the interferometer itself, discussed in section 3 and diagrammed in Figure 5, that arises when beams with differential shear undergo pointing changes. As applied to MAM, this technique is called the “pointing decenter” test. We articulate TA starlight pointing with the FSMs, but this has no effect on the sub-aperture metrology beams, and so a variation in the tip/tilt angle $\Delta\phi$ between the two beams is introduced. This will multiply the shear offset S , that we seek to measure, to produce a recognizable variation in OPD between starlight and metrology, Δd , that is given by $\Delta d = S \cdot \Delta\phi$ (see Figure 5).

For the pointing decenter test, the voice-coil modulator (VCM) is run at 20 Hz with a triangle wave of 2 μm stroke, to permit the basic fringe-fitting that is needed to monitor starlight OPD. At the same time, the FSM in the arm for which starlight and metrology beams are being shear-aligned is run with a slow sinusoidal tip/tilt modulation, with an amplitude of about 1 μrad . The CCD, metrology gauges, and pointing quad-cells are run at 500 Hz. A typical measurement run takes 5 minutes. The shear offset thus

derived ($S = \Delta d / \Delta \phi$) is corrected by moving the pupil mask, which defines the photocenter of the starlight beam. Measurements and pupil mask shifts are iterated until starlight and metrology beams are brought into shear alignment to the desired accuracy.

5. PERFORMANCE METRICS

Field dependency

The errors in the difference between the starlight and metrology on the science interferometer can be divided into two major categories: field independent and field dependent.

- Field independent errors are the same no matter where the instrument is "looking" in the field. For an interferometer, different field locations are achieved by articulating collecting apertures and translating delay lines. A field independent error is independent of where the collecting apertures or the delay line resides. If either of them move, the error is the same. An example of a field independent error is photon noise on a camera.

- Field dependent errors change as a function of location of the articulating collecting apertures and/or translating delay lines. An example is diffraction. This affects the starlight and metrology differently as the delay line translates back and forth on its rails. This difference shows up as an error in the delay determination. However, if the error is constant in time, then it is possible to remove this error through calibration. The error map is measured and then later used as a "look-up" table to correct for the difference between the two. Without the calibration "look-up" table, it is impossible to tell the difference on SIM between the desired delay (signal) and field dependent error (noise).

Field independent errors are of two varieties; random and drift. Averaging reduces the random errors. It does not matter whether the integration time is contiguous or broken up into discrete time periods. Chopping enables the reduction of drift errors. This approach assumes each field point sees the same time dependent error. The drift in the reference star measurement on either side (in time) of a target star measurement is then used to estimate the drift in the target star. This estimate is then removed from the target star value. The chop time is defined by the time constants of the drift errors.

The SIM on-orbit observing scenario includes a field dependent calibration function measurement. This function is then used to "correct" for the field dependent errors on each of the measurements, which will be at various field points. SIM will then make a number of observations, then correct for the field dependent errors by applying the calibration function. The allocated field independent errors and the residual field dependent error post calibration, make up the error allocations validated on MAM. The field dependent calibration function is assumed to be constant

over a long period. This assumption will also be validated on MAM in the MAM environment.

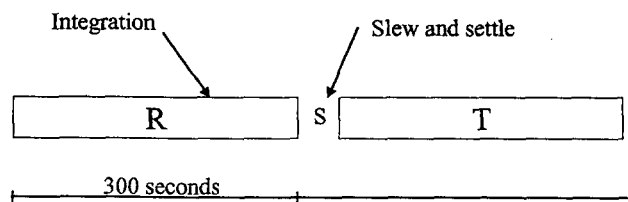
MAM versus SIM basics

SIM uses metrology to measure the difference between white light and metrology in order to determine how much further the star light traveled to one aperture versus the other. The metrology goes through the instrument. In the case of MAM however, metrology goes through the entire instrument, and continues all the way to the pseudo star. SIM's white light/metrology difference signal contains the astrometric delay (the value of interest), field independent errors and field dependent errors of the instrument. In contrast, MAM's white light/metrology difference signal contains the field independent and field dependent errors of both the pseudo star and the instrument. This in fact leads to the fundamental rule of MAM: MAM measures directly the field dependent calibration function for the combined pseudo star /instrument system.

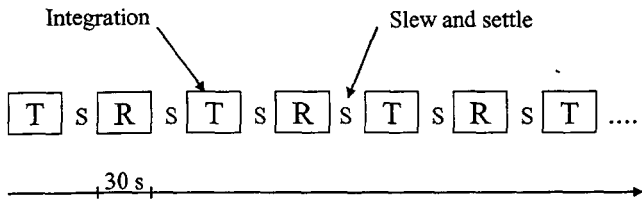
The top-level MAM performance number 150pm (derived from a portion of the SIM narrow angle basic requirement tree) is the combination of the two error terms: field independent and field dependent.

Performance tests

The measurement represents a single SIM narrow angle observation. The definition of a SIM measurement is explicitly defined in the SIM error budget: it involves observing a target star (one suspected to have orbiting planets) for 300 seconds, slewing to one or more reference stars, and observing them for 300 seconds total. The desired quantity is the difference in delays between the target star and the reference star(s).



The integration time per observation for both the reference and the target is limited in order to support the science demands for the entire mission. This however limits the reduction in random noise on the measurement. For example, if there were no limit on integration time, then the random error in the measurement could theoretically approach zero. It is also possible to interleave the reference and target observations in order to remove drift errors. This observing sequence is called "chopping" and its period is dictated by the time constant of the drift errors.



For the field dependent test, the sequence involves moving to multiple field points to emulate the target-reference SIM observing scenario, recording the difference between the white light and metrology through the entire path for 30 seconds, slewing and settling over the next 15 seconds, recording the following 30 seconds of data at the next star position and so on.

The data recorded during a field independent test is simply a long time series of the difference between the white light and metrology through the entire path. The data is then processed as though it was an actual observing sequence. However, that sequence can be parameterized since the target and reference slews are not actually happening. The selected way to process the same data set is to integrate 30 seconds and call that the target star, skip over the next 15 seconds of data to simulate the slew and settle time, to integrate again and call that the reference. Then repeat this sequence 10 times. Note that the total integration time on the target star remained at 300 seconds as did the reference star.

6. DATA ANALYSIS

Raw fringe processing

For the MAM testbed, white light fringes are detected by modulating the optical path via a voice coil in a triangle wave pattern. MAM has the ability to measure the positions of the modulation waveform at picometer accuracy by internal SAVV metrology at 1 kHz rate. The recorded fringe intensity data at each triangle waveform is determined by our CCD camera recording speed, which is 500 frames/sec for our current configuration. For a 25Hz triangle waveform, we record 20 CCD frames (or time bins) during one triangle waveform. We average 2 samples of metrology data to match our camera data. The dither positions are the corresponding averaged positions of SAVV at each CCD frame.

HeNe and white light (which serves as proxy for the star-light) are spectrally dispersed linearly in wave number by the dispersion prism ("spectrometer") onto the 40x40 CCD camera. A single recorded frame from a 40x3 sub-region of the 40x40 camera is shown in Figure 7. White light is dispersed nearly uniformly between 16th (710nm) through 40th (950nm) pixels and HeNe is centered at left on 4th pixel. Dispersed white light on CCD has peak intensity

around 30th pixel, which reflects the intensity peak of our white light source.

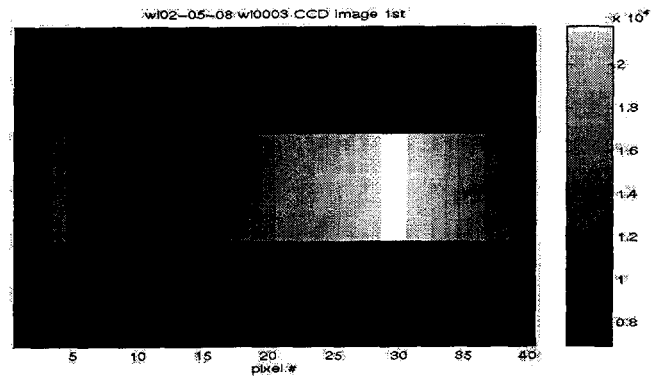


Figure 7 - Dispersed fringe image on the CCD camera showing the HeNe fringe on the left centered on 4th pixel and white light between 16th (710nm) through 40th (950nm) pixels on the right.

For each recorded CCD frame, we co-add the recorded intensity of three rows at each pixel for analysis. Each white light pixel covers between 7.5nm and 11nm of spectral width and hence can be fit for quasi-monochromatic fringes (see eq.(1)). A new fringe-phase measurement is produced every 40 ms for the voice-coil modulator scanning at 25 Hz. A typical HeNe fringe from the CCD and its corresponding dither positions from SAVV are shown in Figure 8. The vibrations and drifts of TA/IIPS, detector noise as well as SAVV noise all will appear in our recorded fringes and hence limit our accuracy in phase delay (or OPD) estimate.

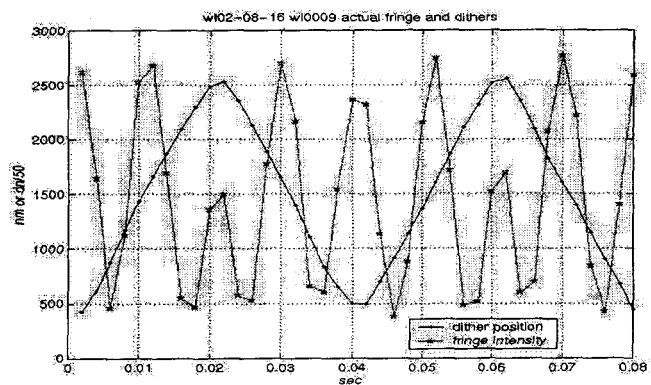


Figure 8 - Actual fringe and dither positions observed in MAM testbed.

Other realizations of fringe plots are shown in Figure 9 and Figure 10. For the HeNe fringes (Figure 9), we had further summed between pixels 2 to 7 in addition to coadding 3 rows on the recorded CCD frame. Each column covers one full dither stroke. Successive strokes are plotted along the horizontal axis, showing good stability over one hour. For the white light fringes (Figure 10), we displayed only one full dither stroke as a function of the spectral. Nearly no tilt of the white light fringe across spectral pixels indicates that

we are at nearly equal path between two interferometer arms during this run.

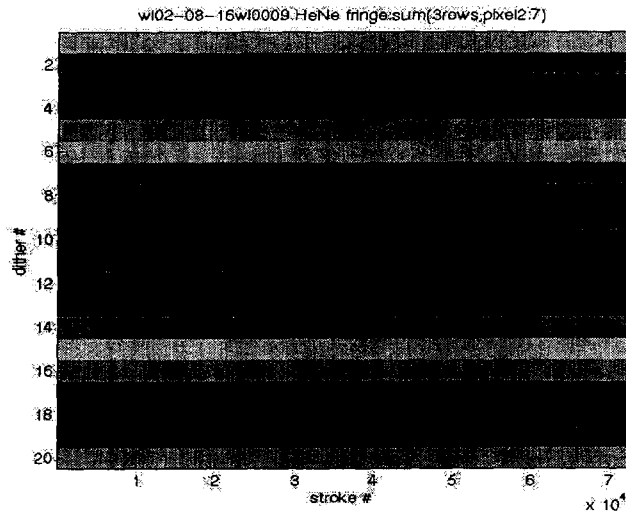


Figure 9 - HeNe fringes from MAM testbed. Each column covers 40 millisecond time span and has 10 dithers for up stroke and 10 dithers for down stroke. 70,000 strokes are plotted along the horizontal axis, showing good stability over one hour

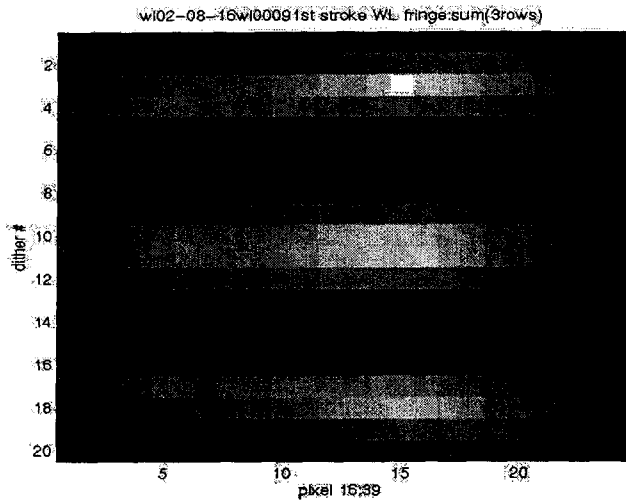


Figure 10 - White light fringes from MAM testbed. We displayed only one 40 msec time stroke, as a function of the spectral channel along the horizontal axis.

Starlight versus metrology path difference

The interference intensity model we used in our algorithms at a given stroke (or scan) is given by:

$$I_{ijl}^{data} = I_{jl} \{ 1 + V_{jl} \cos(k_{jl} x_{ij} + C_{jl}) \}, \quad (1)$$

where l is the index for spectral pixels, j is the index for strokes (or scans), i is the index for dither positions within the stroke. For white light, $l=16, \dots, 39$, which is the spectral pixel index on CCD. I_{jl} , V_{jl} , k_{jl} and C_{jl} are fitted intensity,

visibility, wave number and unknown phase (or delays* wavenumber), respectively, and all assumed to be constant over a given stroke, i.e. over all dither positions x_{ij} at given j, l .

Equation (1) does not include detector noise, power fluctuation or alignment instability within a given stroke. Parameters in Equation (1) can be categorized into system parameters and calibration parameters. These parameters are subject to errors due to light source fluctuations, thermal/tip-tilt/shear drift, vibration, cyclic error, or alignments. The error sources are dominant at different time scales and may be identified by our diagnostic metric. System parameters are intensity, visibility and unknown phase and will be solved by different algorithms. Calibration parameters are pre-calculated white light wave number at each spectral pixel, and measured dither positions.

The white light phase delay is calculated from the mean of equal weighted phase delays at each spectral pixel and is equal to $\langle C_{jl} * \lambda_l / 2\pi \rangle$ where λ_l are calibrated wavelength at l 'th pixel. Measurement accuracy is determined by the accuracy of our OPD, which is the difference between $\langle C_{jl} * \lambda_l / 2\pi \rangle$ and phase measured by SAVV at each stroke. We obtain the white light delay estimate at each stroke using the phase delay rather than group delay, since the available spectral bandwidth of our CCD is narrow in our current MAM setup. Figure 11 shows the optical path difference between white light and metrology (white light phase delay).

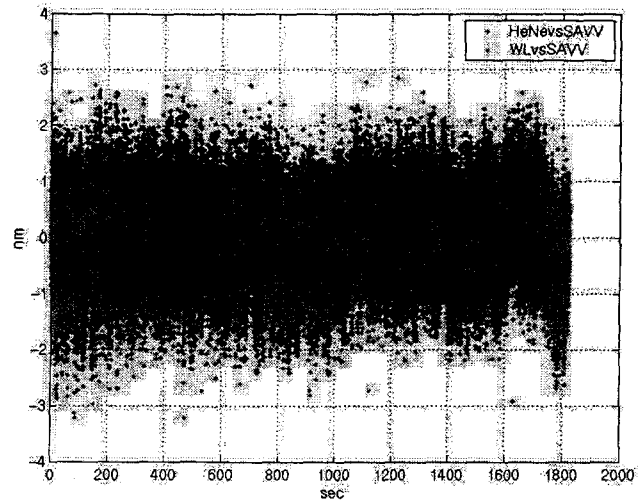


Figure 11 - Example of optical path difference between whitelight and metrology (OPD differences between HeNe and SAVV are shown in the back).

Allan variance to RT deviation (diagnostic tools)

Allan variance⁶ (σ_y^2) is also known as two-sample variance. It is defined as 1/2 of the time mean squares of the differences between successive readings of the data integrated over the integrating period τ and given by:

$$\sigma_y^2(\tau) = 1/2 \langle (\Delta y_i)^2 \rangle \quad (2)$$

where $\Delta y_i = \{y_{i+1} - y_i\}$; averaged samples y_i are taken with no dead-time between them. The y_i is the average of the data y within the i^{th} period τ . In Equation (2), “1/2” makes Allan variance equal to classical variance if the data are taken from white noise. Allan variance has been widely used as a diagnostic tool in frequency standards⁶. Our data y are time series of delay phase (or optical pathlength) differences between white light and metrology.

For the MAM data analysis, we have adopted a modified Allan deviation⁶ and chop deviation⁷ for our diagnostics/performance metrics, based on the observation scenario for SIM chopping back and forward between reference and target stars⁷. The observation scenario representing a single SIM narrow angle observation involves observing a target star (one suspected to have orbiting planets) for 300 seconds, slewing to one or more reference stars, and observing them for 300 seconds total. The desired quantity is the difference in delays between the target star and the reference star(s). In the MAM testbed, we measure all the delays with respect to internal SAVV metrology.

The observation errors are subject to random and systematic (cyclic or drift) noise. Averaging reduces the random errors. It does not matter whether the integration time is contiguous or broken up into discrete time periods. Cyclic errors can be reduced by cyclic averaging or steady pathlength control. Chopping enables the reduction of drift errors. This approach assumes each field point sees the same time dependent error. The drift in the reference star measurement on either side (in time) of a target star measurement is then used to estimate the drift in the target star. This estimate is then removed from the target star value. The chop time is defined by the time constants of the drifts. The chop time should be long enough to minimize random errors and short compared to drift time constant in order to remove drift contributions effectively. The number of allowed chops is determined by the chosen chop time and allowable 300sec total integration time.

The modified Allan deviation, also called RT deviation, is defined as the time standard deviation of differences between successive readings of the R (reference) and T (target) data integrated over the integrating period τ and is given by:

$$\sigma_{yRT}(\tau) = \text{std}(\Delta y_i) \quad (3)$$

where $\Delta y_i = \{y_{i+1} - y_i\}$ with $y_i = R$ (or T) and $y_{i+1} = T$ (or R), respectively. Samples of R and T are, respectively, the averaged delays of reference star and target star over the integration period and taken with no dead time between them in RT deviation. We have eliminated the factor of “1/2” used in Equation (2). RT deviation will be our diagnostic tool in MAM and SIM for field independent errors. The RT deviation is given in Figure 12 for the same run. The minimal of RT deviation is reached around 30 sec.

Note that the last data point is always close zero by definition (see Equation (3)).

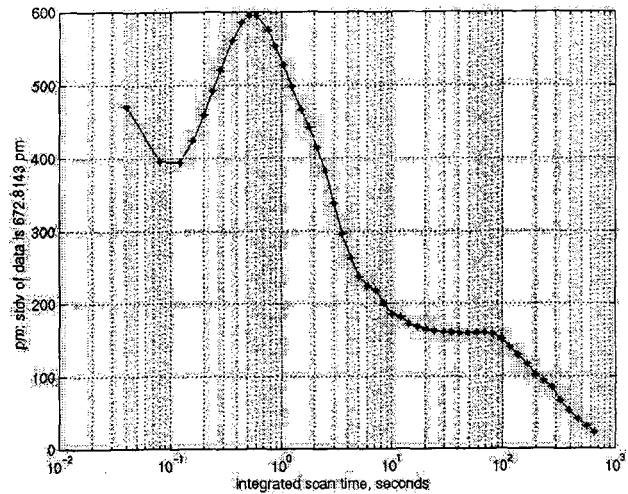


Figure 12 - RT Allan deviation of the optical path difference between white light and SAVV for the same run as Figure 11.

Chop deviation (performance metrics)

Chop deviation (also known as RT chop deviation) is defined as the time standard deviation of the differences between successive R (reference) and T (target) readings of the delays integrated over the period τ with dead time (or slew time) t and is given by

$$\sigma_{ychop}(\tau) = \text{std}(\Delta y_{ichop}) \quad (4)$$

where $y_{ichop} = R_i - T$ is the 1st difference between the averaged delays of target and reference stars during integration period.

Chopping makes SIM immune to many “drift” type error sources. Chop deviation vs. number of chops at a chosen integration time is a predictor of performance, not a diagnostic tool for identifying error sources. In our chopping analysis of quasi-static tests, we adopted an integration time of $\tau = 30$ sec on target and reference, and a dead “slew” time of $t = 15$ sec between target and reference measurements to be consistent with SIM requirements. We have 10 chops with 30 second integration time within 300 second observation time. The chop deviation is given in Figure 13 for the same run.

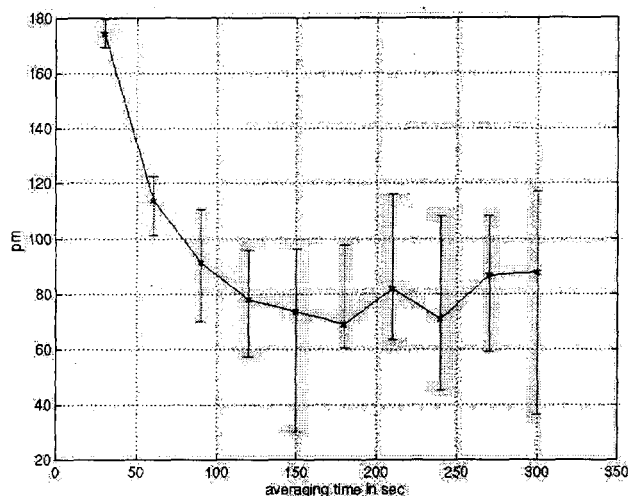


Figure 13 - Chop deviation of optical path difference between white light and SAVV for the same run as Figure 11 and Figure 12.

7. RESULTS

The goal for MAM was to show agreement between metrology and starlight to 150pm. This was tested in three phases. In the first phase, the star was static. In that case, the only error observed was the field independent error. This error has to be reduced to less than 150pm. The second phase is to show the repeatability of our pseudo-star and our ability at keeping the precision alignment when the start articulates from one star position, to another one, back to the initial one. This series of tests is called "go and come back tests". Again the repeatability of the star in terms of error between starlight and metrology has to be better 150pm. The third and final phase is the field independent tests where the pseudo-star periodically articulates from the target star to the two reference stars. For that test, we want to show that the error between starlight and metrology is smaller than 150pm once we removed the systematic field dependent linear calibration error.

Field independent test results

The most useful tool for expressing the performance of MAM in the static field independent mode is the RT Allan Variance. The Allan variance assesses the mean-square error in the difference between OPD measured by the starlight interferometer and OPD measured by the metrology gauge as a function of the time interval over which the data are averaged. It takes into account the temporal structure of the noise, which SIM will also do by strategically interleaving multiple chopped observations of target and calibration stars. Allan variance plots also have diagnostic value, as many common noise mechanisms with characteristic power-law signatures have corresponding characteristic slopes on an Allan variance plot. Our definition takes one-half the

mean square of the differences between successive averaging bins of duration t , and this quantity is plotted against t . For any given astrometric performance level required of SIM, an equivalent performance level for MAM, in picometers of OPD difference, may be derived. So the progression of the MAM experiment has been to push the noise minimum to ever lower levels, in picometers, and to make sure that it occurs on a time-scale suitable for realistic SIM chopping cycles.

In Figure 14 and Figure 15, we show modified Allan variance plots for MAM [10]. Figure 14 represents the performance of the system with coarse alignment only. To calculate this pseudo-Allan variant, the data are divided into contiguous portions of equal duration. The vertical axis is the standard deviation of the average value for each successive portion (with the linear drift removed). The horizontal axis is the time interval into which the data are binned (the integration time). The first point is the standard deviation of the raw data; the last point is zero by definition, being the standard deviation of only two binned-data averages with the linear drift removed.

At short periods (0.1 s to 1 s), the performance is limited by random noise, such as vibration, electronic and photon noise. At long periods (10 s to 100 s), the performance is limited by thermal drifts. After 200 s, the data should be ignored because the standard deviation is evaluated from very few samples. The best performance (350 pm) is obtained for a binning interval of about 0.5 s, and when this interval exceeds a few seconds the performance decreases because of the lack of precision alignment.

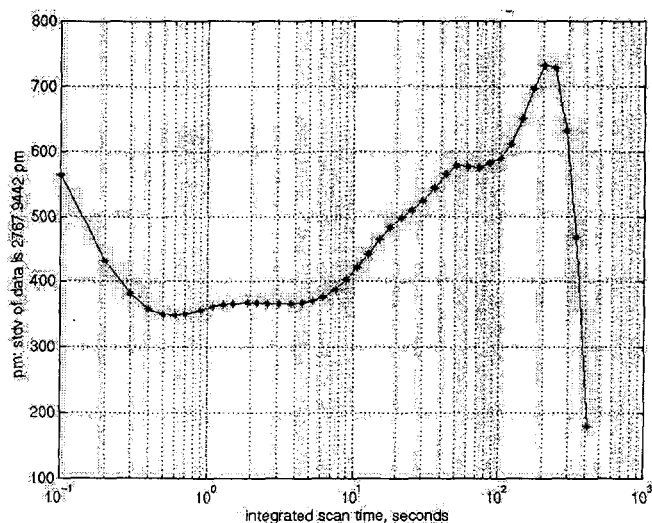


Figure 14 - RT Allan variance prior to precision alignment, June 26, 2002

Figure 15 shows the performance obtained on September 20, 2002, after the precision alignment described in this paper. At short periods (0.1 s to 10 s), the performance keeps on improving with the integration time until we reach the 75 pm minimum at about 15 s. The drift is still present at longer

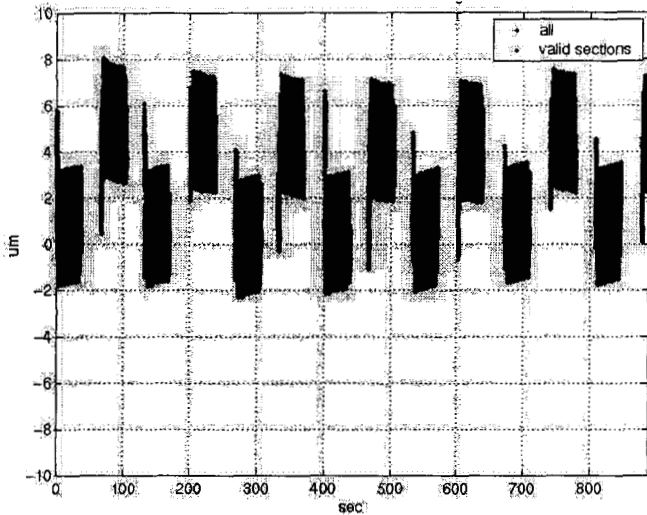


Figure 19 – Delay line position as measured by the metrology during the "go and come-back" test. The valid part of the data after each slew is highlighted.

The first processing step is to select only the valid part of the data, i.e. remove the 30 second slew between each observation. Then, the error between the pathlength estimated from the starlight and from the metrology is processed as described in the previous section. Figure 20 shows the time capture of the error between metrology and starlight on the valid portion of the data.

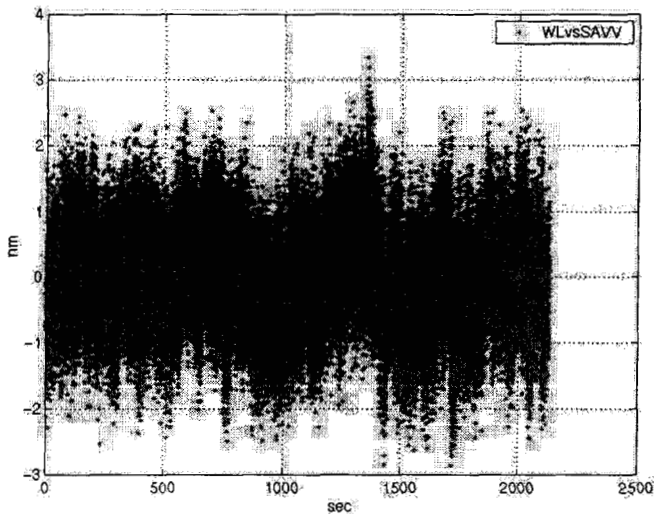


Figure 20 – White light versus metrology OPD for the "go and come back" test after removal of the slew.

Then, for each 30 second observation, the error between starlight and metrology is averaged down to a single number. Figure 21 shows the average value for each of the chops.

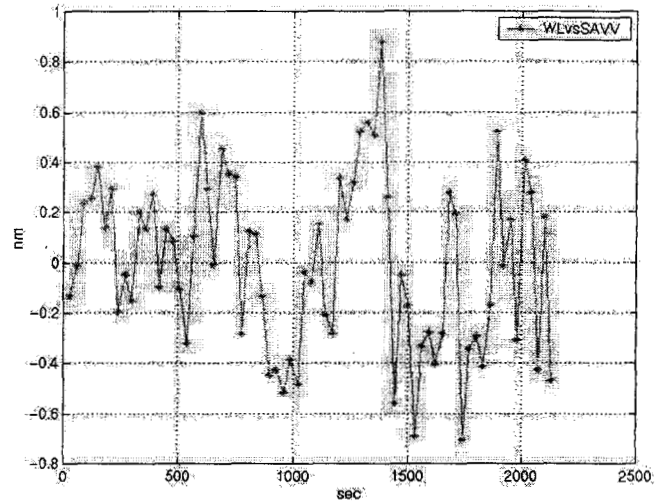


Figure 21 – Relative position of the stars in term of error between starlight and metrology for the "go and come-back" test.

Finally, from the averaged value for each chop, we calculate the rms error as a function of the number of chopped values averaged together. Figure 22 shows the error between white light and metrology paths as a function of the number of chops averaged together. In the SIM scenario, the central star is observed 10 times, therefore the final metrics is the rms error for the 10 chop-averaging. From Figure 22, we measure 110 picometers.

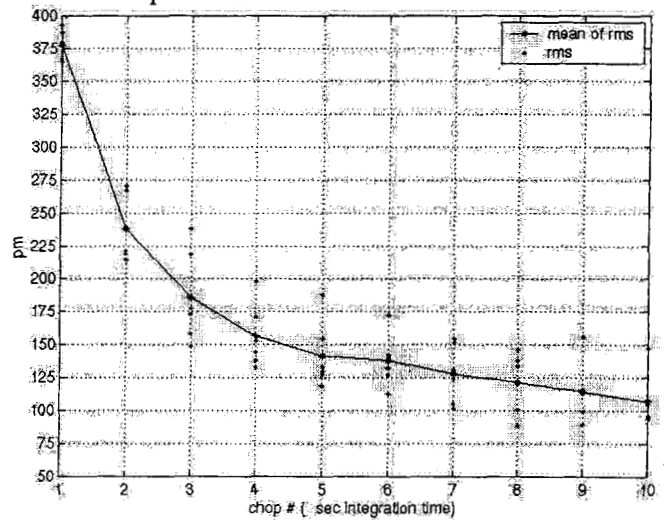


Figure 22 – Error between white light and metrology paths as a function of the number of chops averaged together for the "go and come back" test.

Three-star field dependent test results

Figure 24 shows data taken on October 3, 2002. For this run, we used the "Three star field dependent" sequence (Figure 23). The sequence is 30 seconds of observation time at the target star, followed by 30 seconds to slew to the reference star and 30 seconds of observation time again. Then we slew again back to the same target star, and observe 30 seconds. Finally, we slew to the other reference star (on the opposite

side from the target star, we observe 30 seconds, and slew back to the target star and repeat the sequence from the beginning.

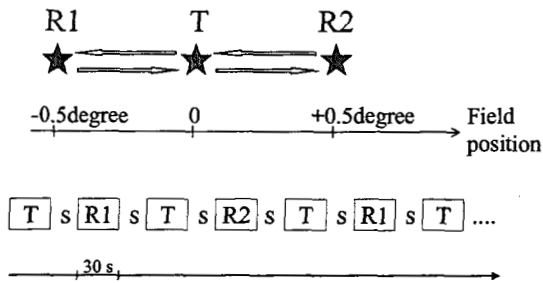


Figure 23 - "Three star field dependent" sequence.

One can see on Figure 24 the two reference stars at +/-28mm on each side of the target one.

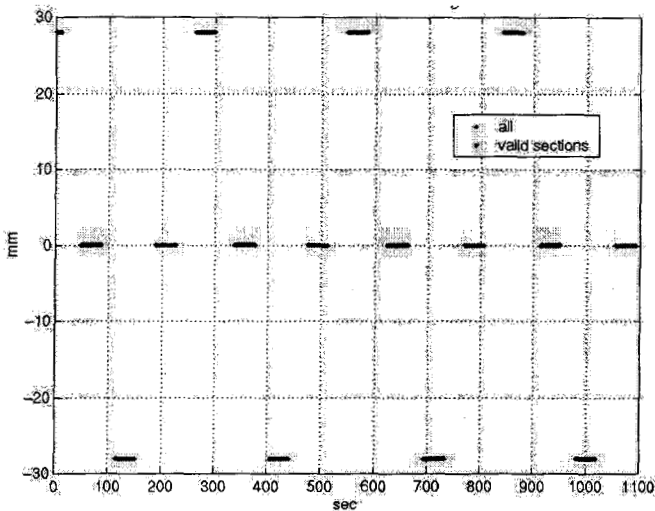


Figure 24 – Delay line position as measured by the metrology during the 3 star field dependent test. The valid part of the data after each slew is highlighted. One can see the two reference stars on each side of the target one.

Again, the first processing step is to select the valid part of the data and then to calculate the error between the pathlength from the starlight and from the metrology sensors. Figure 25 shows the time capture of the error between metrology and starlight on the valid portion of the data. The first star in the sequence is the target star. One can see the two reference stars on each side of the target one in terms of calibration error at the nanometer level.

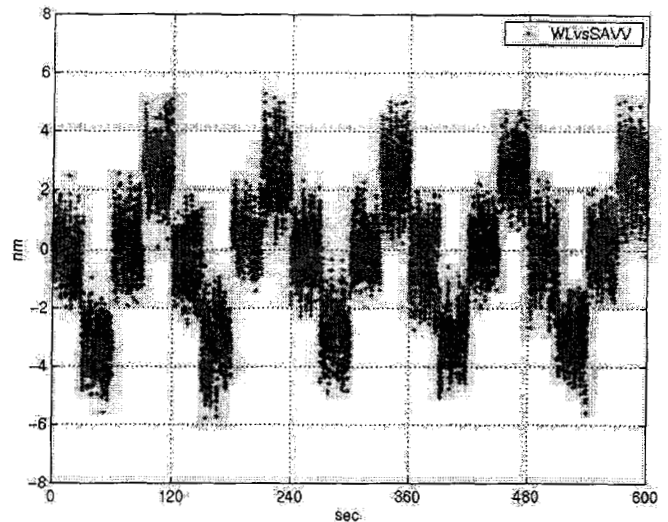


Figure 25 – White light versus metrology OPD for the three star field dependent test after removal of the slew. The first star of the sequence is the target star. One can see the two reference stars on each side of the target one.

Again for each 30 second observation, the error between starlight and metrology is averaged down to a single number. For each chop, we calculate the difference between the calibration error value at the reference and the target star. Figure 26 show the calibration offset between the target and the first reference star at about +1.5 nm and the calibration offset between the target and the second reference star at about -1.5 nm. In fact, we expect the two calibration offsets to be opposite since the two reference stars are located exactly in opposite directions from the target star. Therefore, the mean value of the two calibration offsets is the error of the measured process plus the non-linear portion of the calibration curve. In this test, it is very closed to zero, since the calibration curve is very linear in the narrow angle field of view of MAM (+/-0.5 degree),

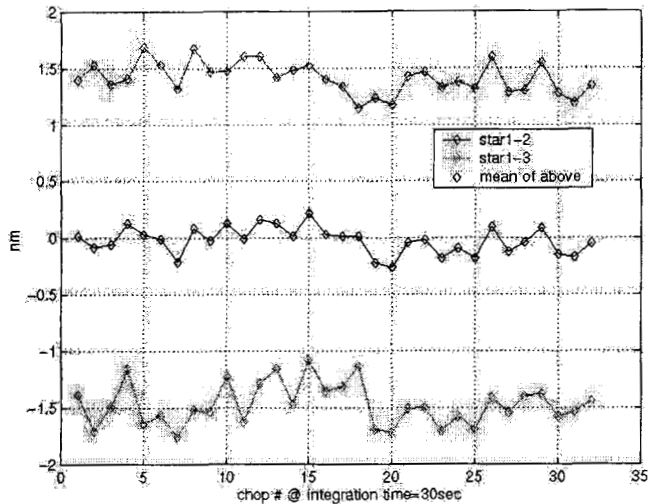


Figure 26 – Relative position of the three stars in term of error between starlight and metrology for the field dependent test. One can see the 3 nm field dependent error between the target and each reference star.

Figure 27 shows the rms error of the linear calibration (middle curve of Figure 26) as a function of the number of chopped values averaged together. In the SIM scenario, the target star is observed 10 times, therefore the final metrics for MAM is the rms error for the 10 chop-averaging. From Figure 27, we measure 80 picometers rms calibration accuracy of the MAM interferometer over its narrow field of view.

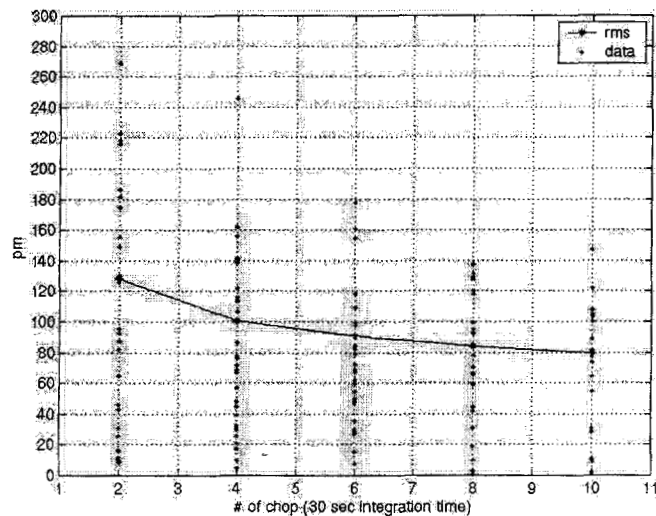


Figure 27 – Error between white light and metrology paths as a function of the number of chops averaged together for the field dependent test (the linear field dependent error has been removed).

8. CONCLUSION

We have discussed some of the critical errors incurred by the MAM testbed for SIM that arise from slight

misalignments of the optics, and have presented a systematic procedure for bringing them into the range required by MAM's error budget. Recent static data taken with the MAM testbed have validated the alignment approach. The alignment scheme for SIM will be based in large part on our experience with MAM. Then we have described the test sequence to assess the performance of the system in the static mode and in the narrow-angle field of view of SIM. We shows less than 20 picometers rms static performance after 300 seconds of observation and about 85 picometers of accuracy between the stars after the linear calibration of the field dependent errors.

ACKNOWLEDGEMENTS

The research described in this publication was performed at the Jet Propulsion Laboratory of the California Institute of Technology, under contract with the National Aeronautics and Space Administration. The results presented are the fruits of an entire team. In particular, the authors would like to thank Dennis Lapicz and Robert Irigoyen for setting up all the sensors and for helping in the laborious alignment.

REFERENCES

- [1] J. Marr, "Space Interferometry Mission (SIM) overview and current status," *SPIE conference on Interferometry in Space*, vol. 4852, 2002.
- [2] R. A. Laskin, "SIM technology development overview - light at the end of the tunnel," *SPIE conference on Interferometry in Space*, vol. 4852, 2002.
- [3] G.W. Neat, James W. Melody, and B.J. Lurie, "Vibration Attenuation Approach for Spaceborne Optical Interferometers," *IEEE Transactions on Control System Technology*, vol. 6, no. 6, pp. 689-700, Nov. 1998.
- [4] R. Goullioud, O.S. Alvarez-Salazar, and B. Nemati, "Dim star fringe stabilization demonstration using pathlength feed-forward on the SIM Test-Bed 3 (STB3)," *SPIE Conference on Interferometry in Space*, vol. 4852, 2002.
- [5] B. Nemati, "External Metrology Truss Technology Demonstration (KITE)," *SPIE Conference on Interferometry in Space*, vol. 4852, 2002.
- [6] B. E. Hines, C. E. Bell, R. Goullioud, R. Spero, G. W. Neat, T. J. Shen, and E. E. Bloemhof, "Micro-arcsecond metrology (MAM) testbed overview," *SPIE conference on Interferometry in Space*, vol. 4852, 2002.

[7] F. Zhao, R. Diaz, G. M. Kuan, N. Sigrist, Y. Beregovski, L. L. Ames, K. Dutta, "Internal metrology beam launcher development for the space interferometry mission," *SPIE conference on Interferometry in Space*, vol. 4852, 2002.

[8] D. B. Schaechter, P. Perkins, C. Tischhauser, D. A. Swanson, R. S. Benson, T. B. Andersen, P. V. Mammini, "Diffraction testbed and results," *SPIE conference on Interferometry in Space*, vol. 4852, 2002.

[9] R. P. Korechoff, "MAM beam walk sensitivities," *JPL Interoffice Memo*, Dec. 10, 2001.

[10] T. J. Shen, M. H. Milman, G. W. Neat, J. Catanzarite, "Dependence of the micro-arcsecond metrology (MAM) testbed performance prediction on white light algorithm approach", *SPIE conference on Interferometry in Space*, vol. 4852, 2002.

[11] G. W. Neat, "The Micro-Arcsecond Measurement testbed and its relationship to the Space Interferometer Mission", *SPIE conference on Interferometry in Space*, vol. 4852, 2002.

Dr. Renaud Goullioud has an engineering degree (1994) in electronics from the Institute of Chemistry and Physics of Lyon (France) and a Ph. D. in micro-electronics. He has been working at JPL in the Interferometry Technology Program since 1997, as an optical engineer. He has developed several optical test-beds related to the SIM mission. Since 2000, he has been the lead of the SIM Test-Bed 3. In 2001, he took the additional responsibility of the optical integration of SIM's Micro-Arcsecond testbed.

